JOURNAL OF GEOPHYSICAL RESEARCH, VOL. 107, NO. D8, 10.1029/2001JD000373, 2002

On the surface and atmospheric temperature changes following the 1991 Pinatubo volcanic eruption: A GCM study

Fanglin Yang[1] and Michael E. Schlesinger

Climate Research Group, Department of Atmospheric Sciences, University of Illinois at Urbana-Champaign, Urbana, Illinois, USA

Received 16 January 2001; revised 19 October 2001; accepted 19 October 2001; published 30 April 2002.

[1] Ensemble numerical simulations are performed using an atmospheric general circulation model to study the responses of the atmosphere to volcanic aerosol forcing and sea surface temperature (SST) forcing during the two years following the Pinatubo eruption. The simulated surface air temperature (SAT) anomalies, forced respectively and jointly by the Pinatubo aerosol and the observed SST anomalies, are compared to those derived from observations using a singular value decomposition (SVD) model. The simulated land SAT anomalies, forced only by the observed SST anomalies, match well in magnitude and time the leading mode of SAT anomalies from the SVD analysis, which represents the ENSO-forced SAT variations. When forced by both the Pinatubo aerosol and the observed SST anomalies, the model captures the observed surface cooling over land in June–July–August and September–October–November 1992 but misses the surface warming over northern Eurasia in December–January–February (DJF) 1991–1992 and DJF 1992–1993. In the atmosphere the simulated temperature anomalies in the troposphere (stratosphere) forced by the Pinatubo aerosol are sensitive (insensitive) to the initial conditions and the type of prescribed SST. The signal of SST forcing is stronger in the troposphere and near the surface than in the stratosphere, while the signal of the Pinatubo aerosol forcing is strongest in the lower stratosphere. The simulated global-mean stratospheric temperature anomalies induced by the Pinatubo aerosol are generally 1°C to 1.5°C larger than observed. Empirical data analyses and numerical model simulations showed that this discrepancy is explained in part by the influences of the quasi-biennial oscillation and the observed ozone depletion, which the ensemble numerical simulations did not resolve. *INDEX TERMS:* 0370 Atmospheric Composition and Structure: Volcanic effects (8409); 1620 Global Change: Climate dynamics (3309); 3359 Meteorology and Atmospheric Dynamics: Radiative processes; 4255 Oceanography: General: Numerical modeling; *KEYWORDS:* Pinatubo, volcano, aerosol, ENSO, temperature

1. Introduction

[2] The impact of volcanic eruptions on the Earth-atmosphere system is multifold. In general, during a volcanic eruption a large amount of SO_2 injected into the stratosphere is converted into H_2SO_4 vapor by OH oxidation. Saturated H_2SO_4 vapor condenses to form aerosol particles (H_2SO_4/H_2O solution). These aerosol particles interact with other aerosol particles in the stratosphere and grow through further condensation, homogeneous and heterogeneous nucleation, and coagulation. They also evaporate when the H_2SO_4 vapor becomes unsaturated. Depending on their size and atmospheric conditions, these aerosol particles can stay in the stratosphere for a few days up to several years before they fall into the troposphere under gravitational settling. In the troposphere the aerosol particles are often washed out quickly by precipitation and eventually come down to the Earth's surface.

[3] Volcanic aerosol particles in the stratosphere can cause large perturbations to the atmospheric chemical constituents and radiation budget [*Robock*, 2000]. For instance, the enhanced heterogeneous reactions on the surface of aerosol particles can convert more reactive nitrogen into inactive nitric acid and lead to an enhancement in the concentration of reactive chlorine, thereby leading to the increased ozone destruction often observed in the stratosphere after volcanic eruptions [*McCormick et al.*, 1995]. Volcanic aerosol particles can disturb the atmospheric radiation budget by reflecting solar radiation, primarily in the ultraviolet (UV) and visible bands, back into space and by absorbing terrestrial radiation and part of the solar radiation in the near-infrared region. The disturbance to the radiation budget causes changes in atmospheric temperature and circulation. The reflection of solar radiation by aerosol particles also increases the photodissociation rates of certain chemical reactions in the stratosphere above the aerosol cloud because of the increased solar UV radiation and thus leads to decreases in the concentrations of several chemical compounds such as ozone [*Tie et al.*, 1994]. Furthermore, the change in the atmospheric circulation modifies the transport and, consequently, the distribution of volcanic aerosol particles over the globe. All these processes are linked to each other and create a complex picture of how volcanic eruptions affect the Earth-atmosphere system.

[4] The Mount Pinatubo volcanic eruption, which occurred on the island of Luzon (15°N, 120°E), Philippines, in June 1991, injected about 20×10^{12} g (20 Tg) of gaseous SO_2 into the stratosphere. The maximum mass loading of stratospheric sulfate aerosol, which was converted from SO_2, was about 30 Tg in the last few months of 1991 [*McCormick et al.*, 1995], more than 30 times as much as the background sulfate-aerosol mass loading. The Pinatubo aerosol particles were transported to high latitudes and

[1]Now at Climate Prediction Center, National Centers for Environmental Prediction, Camp Springs, Maryland, USA.

0148-0227/02/2001JD000373$09.00

suspended in the atmosphere for several years and caused the largest aerosol perturbation to the stratosphere in the 20th century. The Pinatubo eruption has also been the best-observed major volcanic eruption on record [*Russell et al.*, 1996]. It provided us a rare opportunity to better understand the natural variability of the climate system and human-induced climate changes and to test various dynamical, radiative, and chemical models.

[5] There have been three major fields of study on the Pinatubo eruption. The first is focused on the formation, growth, and deposition of the Pinatubo aerosol particles and the chemical effect of these aerosol particles on atmospheric constituents [e.g., *Kinnison et al.*, 1994; *Tie et al.*, 1994; *Zhao et al.*, 1995; *Pudykiewicz and Dastoor*, 1995; *Knight et al.*, 1998]. The second is on the optical properties of the aerosol particles and the radiative forcing these particles imposed on the Earth-atmosphere system [e.g., *Stowe et al.*, 1992; *Minnis et al.*, 1993; *Russell et al.*, 1996; *Stenchikov et al.*, 1998; *Andronova et al.*, 1999]. The third is on the atmospheric responses to the forcing, namely, changes in atmospheric temperature and circulation [e.g., *Groisman*, 1992; *Hansen et al.*, 1992; *Graf et al.*, 1993; *Kirchner and Graf*, 1995; *Robock and Mao*, 1995; *Parker et al.*, 1996; *Kirchner et al.*, 1999; *Ramachandran et al.*, 2000].

[6] This paper is focused on the numerical simulations of the surface and atmospheric temperature changes induced by the Pinatubo eruption. The volcanic and sea surface temperature (SST) signals in the simulated temperature anomalies are separated as in our earlier paper, which analyzes the observed surface air temperature (SAT) anomalies following the Pinatubo eruption [*Yang and Schlesinger*, 2001]. The analysis focused on the identification and separation of the signals of the Pinatubo aerosol and El Niño-Southern Oscillation (ENSO) events in the observed SAT anomalies over land using composite and singular value decomposition (SVD) analyses.

[7] In section 2 we briefly describe the radiative forcing and anomalous radiative heating caused by the Pinatubo aerosol. The reconstruction of the Pinatubo aerosol optical properties and calculation of radiative forcing are found in the work of *Andronova et al.* [1999]. In section 3 we analyze the observed atmospheric temperature changes. The design and results of ensemble numerical simulations are presented in section 4. In section 5 we examine the influences of the quasi-biennial oscillation (QBO) and the observed ozone depletion on the observed and simulated temperature changes following the Pinatubo eruption. A summary is given in section 6.

2. Radiative Forcing and Anomalous Radiative Heating

[8] Though the Pinatubo eruption has been the best observed in history by satellites and ground-based observation stations, the observed database on its own is still not adequate enough in time and space for global studies [*Russell et al.*, 1996]. An accurate description of the aerosol mass loading and optical properties (extinction efficiency, single-scattering albedo, and asymmetry factor) is vital for atmospheric general circulation models (GCM) to correctly calculate the radiative forcing and to simulate the atmospheric responses to the forcing. Using data derived from SAGE-II, UARS, balloon, and lidar observations, together with a Mie-scattering model, *Stenchikov et al.* [1998] developed a time-dependent, zonally averaged, vertically resolved spectral data set of the Pinatubo aerosol optical properties for the ECHAM4 GCM, covering the time from June 1991 to May 1993. They then computed the radiative forcing of the Pinatubo eruption. This data set was also used by *Kirchner et al.* [1999] to simulate the climatic impact of the Pinatubo eruption. A similar data set was also constructed by *Ramachandran et al.* [2000] to simulate the radiative impact of the Pinatubo eruption using the Geophysical Fluid Dynamics Laboratory SKYHI GCM.

[9] The Climate Research Group at the University of Illinois at Urbana-Champaign (UIUC) also constructed a new data set of the Pinatubo aerosol optical properties using the techniques of *Stenchikov et al.* [1998], but based on the radiation spectral bands and spatial structure of the UIUC 24-layer stratosphere-troposphere (ST) GCM [*Yang et al.*, 2000], and calculated the instantaneous radiative forcing of the Pinatubo aerosol [*Andronova et al.*, 1999; *Yang*, 2000]. *Andronova et al.* [1999] used the calculated forcing of the Pinatubo eruption together with the optical depths of historical volcanic eruptions complied by *Sato et al.* [1993] to reconstruct the radiative forcing of historical volcanic eruptions from 1850 to 1994. Readers are referred to *Andronova et al.* [1999] and *Yang* [2000] for the reconstruction of the optical data and the calculation of the radiative forcing. Here we briefly describe the globally averaged radiative forcing.

[10] Figure 1 shows the global monthly mean instantaneous radiative forcing from June 1991 to May 1993 for the terrestrial (longwave) radiation, solar radiation in the near-infrared band (0.7 μm–10 μm), and the UV and visible band (0.175 μm–0.7 μm), and the total (terrestrial plus solar). Forcings are calculated under both clear-sky and cloudy-sky (all) conditions at the model top (1 hPa), tropopause and the Earth's surface. The forcing in the solar near-IR band at the model top and tropopause is as large as that in the UV and visible band but 1.0–1.5 W/m^2 smaller at the Earth's surface. This results from the absorption by water vapor in the solar near-IR band in the troposphere. The Pinatubo aerosol cloud was located in the lower stratosphere. Because the average atmospheric emitting temperature is higher for layers below the aerosol cloud than above it, the longwave forcing at the model top (1 hPa) is much larger than that at either the Earth's surface or the tropopause. At the model top, the largest total forcing is found at the end of 1991 and in early 1992, about −7 W/m^2 under clear sky and −4.7 W/m^2 under cloudy sky. The presence of clouds reduced the radiative forcing of the Pinatubo aerosol.

[11] The radiative forcing simulated by the UIUC ST-GCM is generally larger than that simulated by the ECHAM4 GCM [*Stenchikov et al.*, 1998]. *Yang* [2000] showed that under both clear and all-sky conditions the simulated maximum zonal-mean total forcing by the UIUC model is about 2–3 W/m^2 larger in the tropics at the end of 1991 and early 1992 than that simulated by the ECHAM4 model at both the Earth's surface and the tropopause. Among all possible factors, the difference can be attributed primarily to different aerosol optical depths prescribed in these two models. First, the UIUC model overestimated the aerosol optical depth in the tropics compared to the AVHRR observation, while the ECHAM4 model underestimated in the tropics compared to the AVHRR observation and in the middle latitudes compared to both the AVHRR and the SAGE-II observations. The maximum difference of column-integrated optical depth at 0.55 μm averaged over the AVHRR-covered latitudes between these two model estimations is about 0.07 [*Yang*, 2000]. Second, the aerosol prescribed in the UIUC model extends from 200 hPa to 3 hPa, while the one prescribed in the ECHAM model extends from 200 hPa to 10 hPa. Our calculation using a one-dimensional (1-D) column radiative-transfer model shows that given the same column-integrated optical depth, the higher the aerosol clouds extend the larger the total radiative forcing.

[12] The maximum zonal-mean all-sky radiative forcing simulated by the UIUC ST-GCM is also about 3–4 W/m^2 larger in the tropics than that simulated by the SKYHI GCM [*Ramachandran et al.*, 2000]. However, the time-latitude distribution of column-integrated optical depth at 0.55 μm presented by *Ramachandran et al.* [2000] is almost identical to that used for this study [*Andronova et al.*, 1999]. As *Ramachandran et al.* [2000] pointed

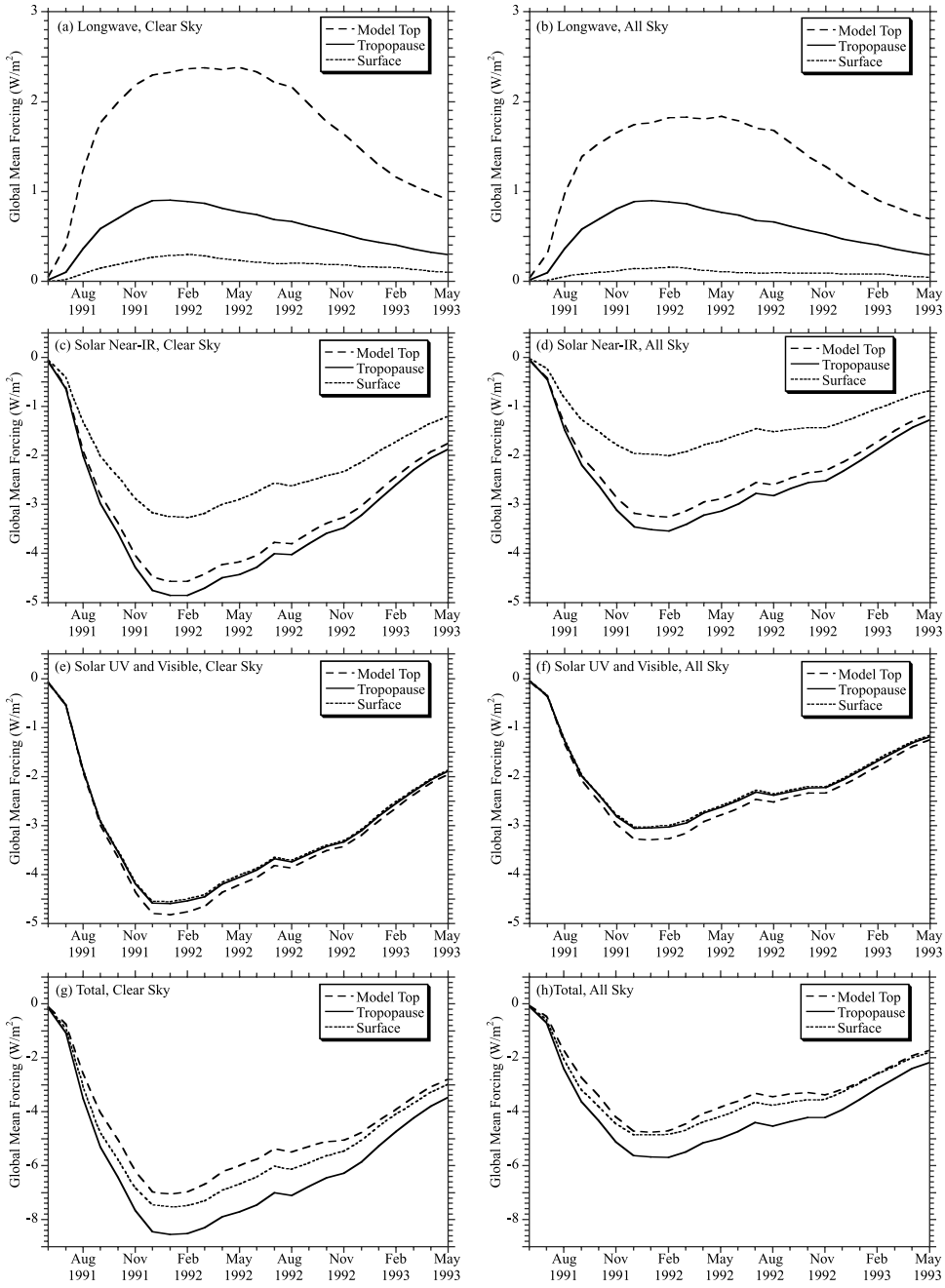

Figure 1. Global-mean radiative forcing at the surface, tropopause, and 1 hPa under clear-sky (left panels) and cloudy sky (right) conditions following the Pinatubo eruption in June 1991: (a, b) longwave radiation; (c, d) solar near-IR radiation; (e, f) solar UV and visible radiation; (g, h) total (solar plus longwave).

out, because of an overestimated cloud amount the attenuation effect on the calculated aerosol radiative forcing by cloud in the SKYHI model is stronger than in both the UIUC and the ECHAM4 models. The clear-sky forcing calculated by the UIUC model is closer to that simulated by the SKYHI model than that simulated by ECHAM4 model, though still larger than SKYHI. It should be pointed out that aerosol clouds in the SKYHI model also extend up to only 10 hPa.

[13] Of course, other differences among these GCMs such as the radiative-transfer algorithms and the simulated water vapor distributions might also be responsible for the aforesaid differences in their simulated aerosol forcing.

[14] To simulate the climatic impact of volcanic aerosol forcing, it is the radiative flux convergence as well as the radiative forcing that matters. As *Ramachandran et al.* [2000] pointed out, the heating and cooling rates of the Pinatubo aerosol simulated by the ECHAM4, SKYHI, and UIUC GCMs are rather close to each other. The Pinatubo volcanic aerosol radiatively cooled the troposphere and radiatively warmed the stratosphere. In January 1992, when the radiative forcing reached its maximum, the maximum cooling was about -0.01°C/d near the surface in the tropics, and the maximum warming was about 0.3°C/d near 30 hPa in the tropics. Until August 1992, the heating rate was still as large as 0.3°C/d near 30 hPa in the

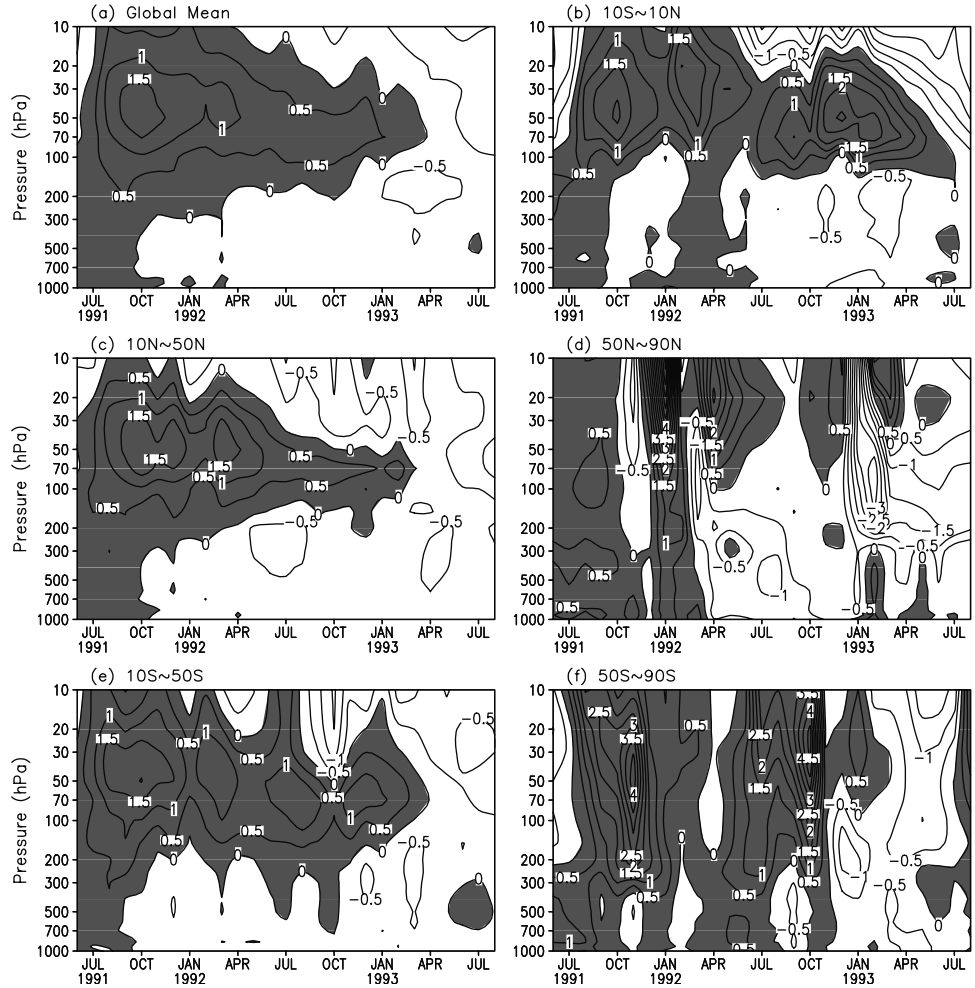

Figure 2. Observed monthly mean air temperature anomalies from June 1991 to August 1993 averaged over (a) the globe and the latitudinal belts among (b) 10°S–10°N; (c) 10°N–50°N; (d) 50°N–90°N; (e) 10°S–50°S; and (f) 50°S–90°S. The contour interval is 0.5°C. Positive anomalies are shaded.

tropics, mainly due to the absorption of longwave radiation by the aerosol cloud [*Yang*, 2000].

3. Observed Atmospheric Temperature Changes

[15] Large SAT changes were observed for a few years following the Pinatubo eruption. *Yang and Schlesinger* [2001] performed composite and SVD analyses to detect and to separate the signals of the Pinatubo aerosol and ENSO events in the observed SAT anomalies. They found that ENSO signals were weak over Eurasia but relatively strong over the other continents. Over North America the 1991–1992 El Niño event contributed more than 50% to the observed total cooling of about −1.0°C in June–July–August (JJA) 1992. Averaged over the four continents, maximum coolings of about −0.5°C occurred in September–October–November (SON) 1992 and SON 1993 with the ENSO signals removed.

[16] Here we analyze the observed atmospheric temperature changes following the Pinatubo eruption using the NCEP/NCAR reanalysis, provided through the NOAA Climate Diagnostics Center. Figure 2 shows the time-altitude cross sections of monthly mean air temperature anomalies from June 1991 to August 1993 averaged over the globe and over different latitudinal belts. The anomalies are relative to the mean of 1979–1995, which coincides with the time period of the SST climatology used in section 4 for the GCM simulations. The anomalies so defined include the trend of temperature changes presumably caused by global warming. During 1979–1995 the global-mean temperature decreased about 0.02–0.03°C/yr in the middle and lower stratosphere and increased less than 0.01°C/yr in the middle troposphere (pictures not shown). The large signal of the Pinatubo eruption makes this trend relatively unimportant. Furthermore, excluding the postvolcano years in the 1979–1995 reference would have made only a 0.1°C difference in global-mean temperature in the middle and lower stratosphere.

[17] Global-mean air temperature increased throughout the atmosphere immediately after the Pinatubo eruption. Large anomalies of about +1.5°C were found in the lower stratosphere between 70 hPa and 30 hPa in SON 1991. After October 1991, tropospheric temperature anomalies became negative. In the lower stratosphere, positive temperature anomalies were observed until March 1993 with gradually reducing magnitudes. In the tropics (10°S–10°N) the warming in the lower stratosphere lasted until July 1993, longer than the warming in the middle latitudes in both hemispheres (10°S–50°S and 10°N–50°N). The magnitude of the warming was also larger in the tropics than in the middle latitudes. A maximum warming in the tropics appeared in DJF 1992–1993, instead of in DJF 1991–1992 immediately after the Pinatubo eruption, because the phase of the QBO changed from easterly before March–April–May (MAM) 1992 to westerly after JJA 1992 (figures not shown). *Angell* [1997b] showed that stratospheric temperature decreases in the tropics during easterly phases of the QBO and increases during westerly phases. At high latitudes (Figures 2d and 2f) the temper-

Table 1. Ensemble Simulations Performed by the 24-Layer ST-GCM

Ensemble Simulations	Prescribed SSTs	Including the Pinatubo Volcanic Aerosol (VOL) ?
E1	CSST	no
E2	CSST	yes
E3	RSST	no
E4	RSST	yes

ature anomalies are of large magnitude and variance. They are related to the dynamical responses of the atmosphere to the anomalous radiative heating at lower latitudes by the Pinatubo aerosol [*Graf et al.*, 1993] and to the observed ozone losses [*Randel et al.*, 1995].

4. GCM Experiments

[18] A few studies have used atmospheric GCMs to investigate the impact of the Pinatubo aerosol on the atmospheric temperature and circulation [e.g., *Hansen et al.*, 1992; *Graf et al.*, 1993; *Kirchner and Graf*, 1995; *Kirchner et al.*, 1999; *Ramachandran et al.*, 2000]. In these earlier studies, little attention was paid to the influence of the observed SST anomalies on the simulated temperature changes induced by the Pinatubo aerosol. Here we use our 24-layer ST-GCM and the aerosol optical data, reconstructed specifically for this model, to study the climatic impact of the Pinatubo aerosol and to separate this impact from that induced by the SST forcing.

4.1. UIUC 24-Layer ST-GCM

[19] The 24-layer ST-GCM was developed mainly on the basis of the UIUC 11-layer atmospheric GCM [*Wang*, 1996; *Wang and Schlesinger*, 1999]. The 24-layer ST-GCM has a horizontal resolution of 4° latitude by 5° longitude. Vertically, the model extends from the Earth's surface to 1 hPa and uses sigma as its vertical coordinate. For a surface pressure of 1000 hPa, there are 10 layers above 100 hPa with constant log-pressure thickness and 14 layers below 100 hPa with prescribed pressure values. *Yang et al.* [2000] has documented the development and performance of the model in detail.

[20] The 24-layer ST-GCM resolves the aerosol radiative forcing explicitly in both the solar and the terrestrial bands [*Yang et al.*, 2000]. Atmospheric chemistry is not considered in any of the following experiments.

4.2. Design of Ensemble Simulations

[21] Using the UIUC 24-layer ST-GCM, we performed four sets of ensemble simulations (Table 1). Each set contains six simulations that use different initial conditions, and each simulation spans two years from June 1991 to May 1993. These initial conditions were randomly chosen from a 15-year control run of the model forced by seasonally varying climatological SSTs [*Yang et al.*, 2000]. In Table 1, CSST means climatological monthly mean SST, which is the 17-year average from 1979 to 1995. RSST means real-time monthly mean SST from June 1991 to May 1993. The Pinatubo aerosol was introduced into the model by using the reconstructed aerosol optical data of *Andronova et al.* [1999]. We list in Table 2 the five experiments that we constructed from the four sets of ensemble simulations in Table 1. In the figures that follow, a label is assigned to each experiment starting with SI, which means simulation and is used to distinguish itself from the observational data analyses (OB). Figures for the experiments SI:SSTA and SI:VOL/CSST are not shown since they are, respectively, similar to those for the experiments SI:SSTA/VOL and SI:VOL/RSST. Throughout the paper we define the model anomaly as the difference between each perturbation run and the ensemble average of the corresponding six control runs.

4.3. Simulated SAT Anomalies

[22] *Yang and Schlesinger* [2001] separated the signals of Pinatubo-aerosol and ENSO events in the observed SAT anomalies over land using composite and SVD analyses. Here we compare the simulated ensemble-mean seasonal-mean SAT anomalies with those derived from observations for the time from JJA 1991 to MAM 1993 averaged over the four continents (Eurasia, North America, South America, and Africa) (Figure 3). To show the uncertainties of the results associated with the model's internal variability, seasonal-mean SAT anomalies derived from each individual simulation are also plotted.

[23] The combined effect of the Pinatubo aerosol and SST forcing is shown in Figure 3a, which compares the simulated continental SAT anomalies, forced by both the Pinatubo aerosol and SST anomalies (SI:VOL + SSTA), with the high-pass filter (HPF) observed SAT anomalies having timescales less than 120 months (OB:HPF). Figure 3b demonstrates the effect of the SST forcing by comparing the simulated continental SAT anomalies, forced only by the SST anomalies (SI:SSTA), with the projections of the leading-mode SAT anomalies from the SVD analysis (OB:SVDP1), which is the part of the SAT anomalies explained by the observed SST anomalies in the eastern tropical Pacific. Figure 3c demonstrates the effect of the Pinatubo aerosol by comparing the simulated continental SAT anomalies, forced only by the Pinatubo aerosol (SI:VOL/RSST), with the residuals between OB:HPF and OB:SVDP1, which represents the observed SAT anomalies induced by the Pinatubo aerosol and possibly forcings other than SST. In the experiment SI:VOL/RSST, the observed real-time SSTs are used as boundary conditions in both the control runs and the perturbation runs.

[24] For all three ensemble experiments, the signal-to-noise ratio is usually larger in JJA than in DJF because of a stronger internal variability over the northern continents in DJF. Thus a large ensemble size is needed to obtain statistically significant results. We compare here the simulated ensemble-mean SAT anomalies with observations. Figure 3b shows that when forced only by the SST anomalies, the model simulates rather well the observed global-mean continental SAT anomalies that can be explained by the SST anomalies in the eastern tropical Pacific from the SVD analysis (OB:SVDP1). The simulated ensemble-mean SAT averaged over the four continents increased from JJA 1991 to MAM 1992 by about 0.1°C and decreased from MAM

Table 2. Experiments and Climate Changes Induced by the Pinatubo Aerosol and/or SST Anomalies

Experiments	Differences	Climate Changes Induced by the Following
VOL/CSST	E2 − E1	Pinatubo aerosol simulated with climatological SST
VOL/RSST	E4 − E3	Pinatubo aerosol simulated with real-time SST
VOL + SSTA	E4 − E1	Pinatubo aerosol and SST anomalies
SSTA	E3 − E1	SST anomalies without Pinatubo aerosol
SSTA/VOL	E4 − E2	SST anomalies with Pinatubo aerosol

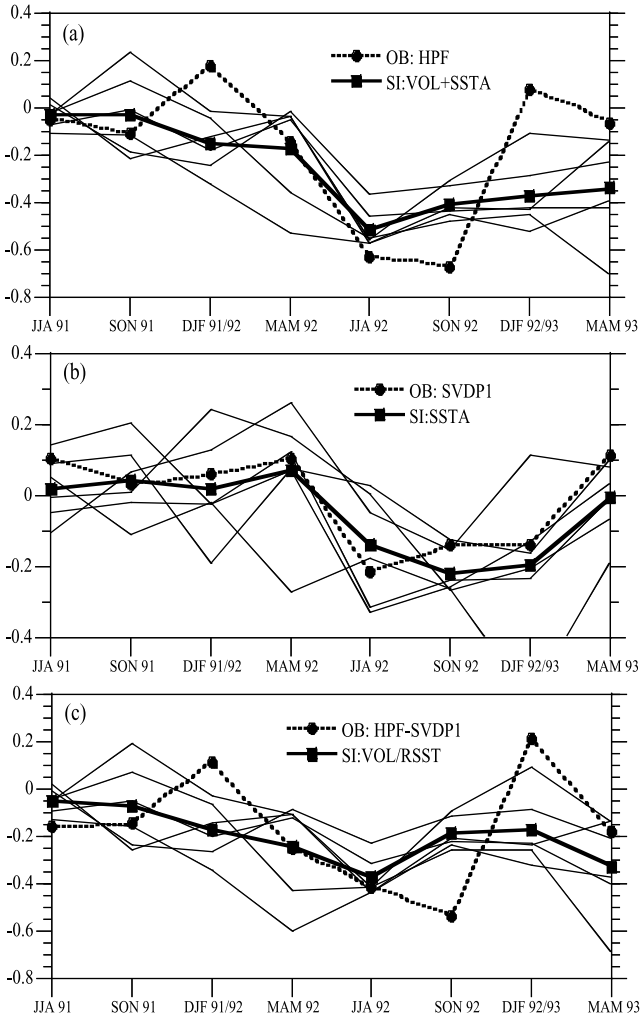

Figure 3. SAT anomalies (°C) averaged over the continents of Eurasia, North America, South America, and Africa for the GCM experiments and SVD analysis forced by (a) both the volcanic aerosol forcing and the SST anomalies, (b) SST anomalies, and (c) the volcanic aerosol forcing. In each panel, dotted lines marked by solid circles show observations from the SVD analysis; thick lines marked by solid squares show the simulated ensemble-mean SAT anomalies; and the six thin lines show results from each ensemble member. See the text and Table 2 for the meaning of the legends.

1992 to SON 1992 by about 0.25°C. Figure 3b also indicates that the SVD analysis is capable of finding the coupled patterns between the continental SAT anomalies and the SST anomalies in the eastern tropical Pacific. When forced by both the Pinatubo aerosol and the SST anomalies (Figure 3a), the model simulates rather well the observed global-mean SAT anomalies in the Northern Hemisphere spring and summer. The SAT averaged over the four continents decreased by 0.5°C in the simulation and by 0.63°C in the observation in JJA 1992, of which 0.14°C in the simulation (experiment SI:SSTA) and 0.21°C in the observation (OB:SVDP1) are due to the SST anomalies. The model did not capture the observed warming in DJF 1991–1992 and DJF 1992–1993, although two out of the six ensemble members do match rather well with the observation. The simulated ensemble-mean SAT anomalies are negative. When forced only by the Pinatubo aerosol (Figure 3c), the model simulates well the observed temperature anomalies in the Northern Hemisphere spring and summer but rather poorly in the Northern Hemisphere fall and winter, regardless of whether climatological (figure not shown) or real-time SSTs are used as the lower boundary conditions.

[25] We further analyze the geographical distributions of SAT anomalies. Figures 4 and 5 are the simulated and observation-derived seasonal-mean land SAT anomalies in DJF 1991–1992 and JJA 1992, respectively. For the simulation, ensemble means with statistical significance at or below the 10% level of a two-tailed *t*-test are shaded. For the observation, areas with values exceeding 1.3σ in magnitude are also shaded, where σ is the standard deviation of the high-pass-filtered seasonal-mean SAT anomalies at each grid point between 1950 and 1997. For a time series with a normal distribution and with no autocorrelation, about 10% of the data fall outside of the range $\{-1.3\sigma, 1.3\sigma\}$. Therefore the shaded areas are at or below about the 10% level of statistical significance.

[26] In DJF 1991–1992 the experiment SI:VOL + SSTA captured the large warming of about 3°C over central and northwestern North America and the cooling over North Africa, where the observed temperature anomalies are statistically significant (Figure 4d). Over central Eurasia the observed anomalies are about +2°C but not statistically significant, and the model-simulated anomalies are negative. For experiment SI:SSTA the simulated SAT anomalies over central North America are about 0.5°C–1.0°C and match the corresponding observations associated with the El Niño/La Niña modes derived from the SVD analysis (Figure 4e). For experiments SI:VOL/RSST the simulated SAT anomalies do not match well the corresponding observational analysis in Figure 4f. In JJA 1992 (Figure 5), all simulations have larger areas of statistically significant SAT anomalies than in DJF 1991–1992. The simulated SAT anomalies generally match the corresponding observations. Over North America, both SST anomalies and the Pinatubo aerosol contributed to the observed cooling. The observed signal of SST anomalies is stronger over North America than over Eurasia.

[27] A few points can be drawn from Figures 4 and 5. First, the simulated SAT anomalies are sensitive to the initial conditions and are not everywhere statistically significant, especially at high latitudes in DJF 1991–1992. Second, the natural variability of the observed SAT at the Northern Hemisphere high latitudes is larger in DJF than in JJA and larger over central Eurasia than over North America. The model performs better in regions where the observed SAT anomalies are significant. In their perpetual-January experiments, *Graf et al.* [1993] showed that when forced by the Pinatubo aerosol, the ECHAM2 GCM produced a stronger-than-normal northern polar-night jet and stronger-than-normal zonal winds extending down to the troposphere. The Azores High was shifted northward with increased tropospheric westerly winds at 60°N and increased easterly winds at 30°N. Surface temperatures were higher than normal over northern Eurasia and North America. However, the version of the 24-layer ST-GCM used for the present simulations did not simulate the Northern Hemisphere polar-night jet well [*Yang et al.*, 2000]. In DJF the zonal-mean zonal wind in the middle to upper stratosphere near the North Pole is about 20 to 30 m/s weaker than observed. At 60°N the westerly winds in the stratosphere decay too early in October and do not intensify and propagate further downward in later months as the observed. This deficiency might have prevented the model from simulating correctly the dynamical responses of the atmosphere to the Pinatubo aerosol forcing near the North Pole in DJF. *Kirchner et al.* [1999] showed, however, that this dynamical effect is difficult to simulate in part because the high sensitivity of a troposphere-stratosphere interaction to the background planetary-wave structure determined by SSTs. Third, the observed surface cooling in the Northern Hemisphere in JJA 1992 was mostly due to the direct radiative effect of volcanic aerosols, i.e., the backscattering of solar radiation. There are fewer model dynamical responses involved in JJA than in DJF.

[28] By applying singular value decomposition (SVD) to observational data, *Yang and Schlesinger* [2001] separated the signals of

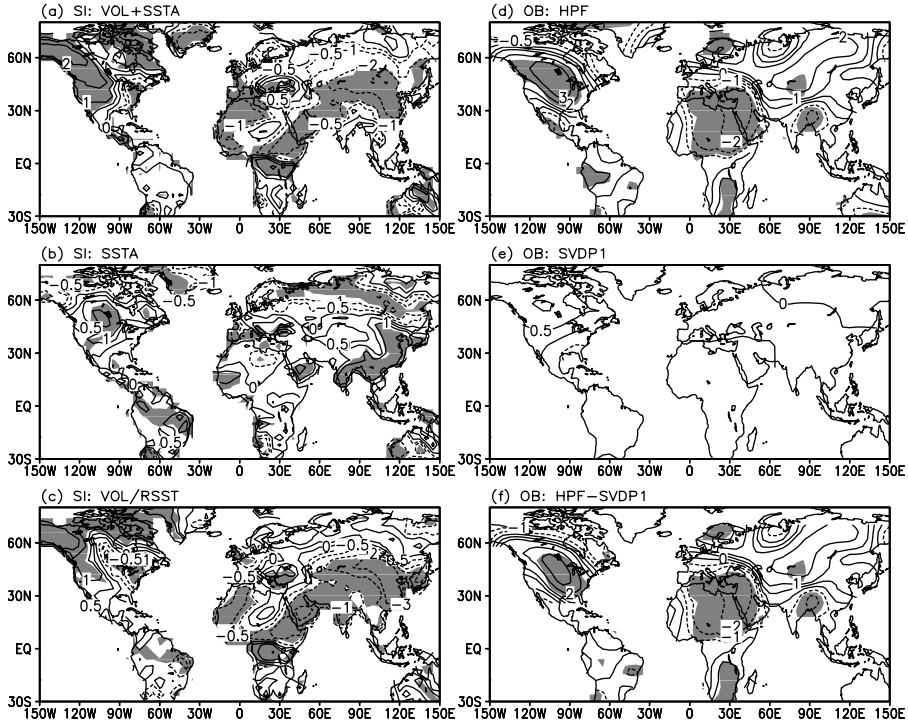

Figure 4. Geographic distributions of SAT anomalies over land in DJF 1991–1992 for (a, b, c) model simulations and (d, e, f) corresponding observations. The contour interval is 1°C with the ±0.5°C lines added. Dashed lines show negative anomalies and solid lines positive anomalies. In Figures 4a, 4b, and 4c, anomalies that are statistically significant at the 10% level for a two-tailed *t*-test are shaded, and in Figures 4d, 4e, and 4f, anomalies larger than 1.3σ in magnitude are also shaded, where σ is the standard deviation of the high-pass-filtered seasonal-mean temperature anomalies at each grid point between 1950 and 1997.

SST and Pinatubo aerosol forcing in the observed surface air temperature. They emphasized the limitations of the linear SVD analysis. First, the atmospheric response to warm-event SST anomalies is stronger than to cold-event SST anomalies, though to the first order, the response is indeed linear [*Kumar and Hoerling*, 1998]. Second, the dynamical response of the atmosphere to the Pinatubo aerosol forcing is sensitive to the background planetary-wave structure determined by SSTs [*Kirchner et al.*,

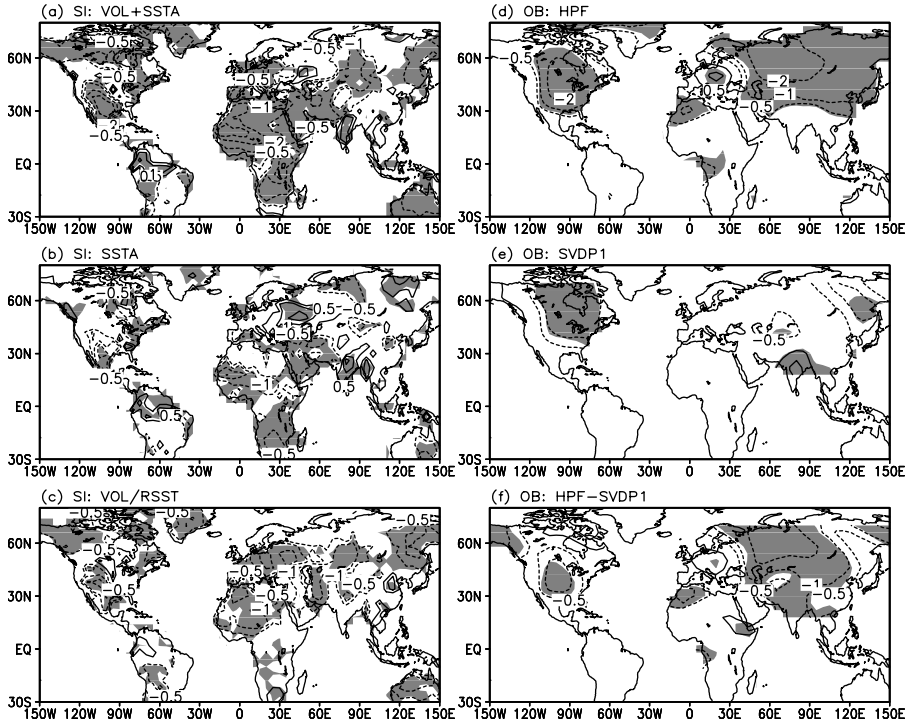

Figure 5. As in Figure 4 except for JJA 1992.

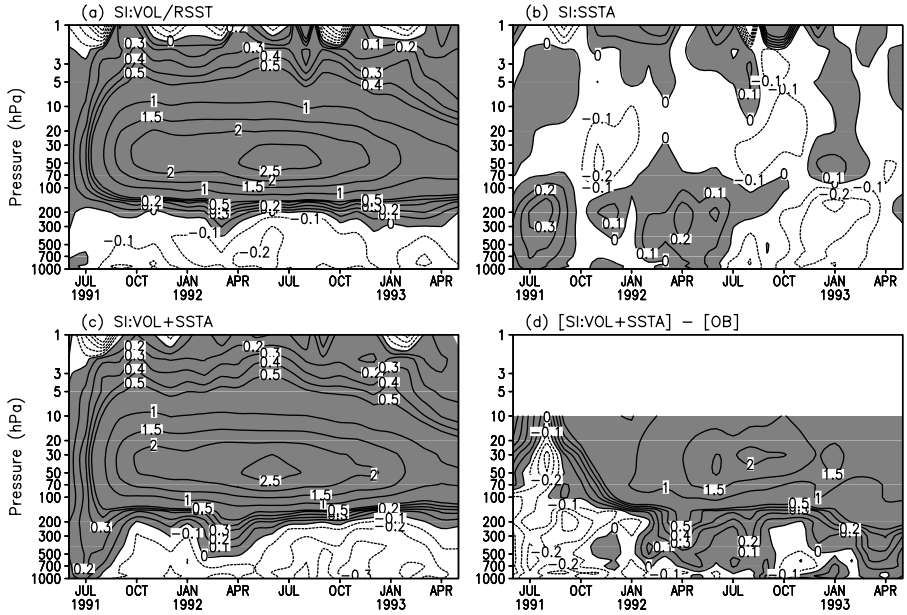

Figure 6. Simulated ensemble-mean monthly global-mean temperature anomalies from the experiments (a) SI:VOL/RSST, (b) SI:SSTA, and (c) SI:VOL + SSTA, as a function of pressure and month following the Pinatubo eruption, and (d) the difference between the experiment SI:VOL + SSTA and the NCEP/NCAR reanalysis. Positive anomalies are shaded. The contour intervals are 0.1 for values between −0.5 and +0.5 and 0.5 for values beyond ±0.5.

1999]. In other words, the dynamical responses to volcanic aerosol and SST forcing may not be linear. In the present study, we performed sensitivity experiments using the UIUC GCM to separate the signals. In principle, any nonlinear response to the combined SST and aerosol forcing is resolved by the model in the experiment (VOL + SSTA) (Table 2). We compared further surface air temperature averaged over all continents derived from experiment (VOL + SSTA) with the summation of those from experiments (SSTA) and (VOL/CSST) and found that the model's response to SST and aerosol forcing is almost linear, especially in the JJA season. Locally, larger nonlinearity is found over northern Eurasia and Alaska. In spite of the limitations, the signal of SST forcing simulated by the GCM matches well with that derived from the SVD analysis.

4.4. Simulated Atmospheric Temperature Changes

[29] Figure 6 presents the global-mean monthly mean temperature anomalies as a function of pressure and month following the Pinatubo eruption for the ensemble experiments SI:VOL/RSST, SI:SSTA and SI:VOL + SSTA, and the difference between the experiment SI:VOL + SSTA and the NCEP/NCAR reanalysis. For each set of ensemble runs, the simulated global-mean temperature anomalies throughout the atmosphere are not sensitive to the initial conditions (figures not shown). We present only the ensemble means in Figure 6 which can be compared to the observed anomalies shown in Figure 2a, albeit noting that they extend only to 10 hPa, while the simulated anomalies extend to 1 hPa.

[30] When the model is forced by the Pinatubo aerosol with real-time SST (Figure 6a, VOL/RSST) as boundary conditions, the simulated temperature increases in the stratosphere and decreases in the troposphere. The experiment SI:VOL/CSST produces almost the same temperature distributions (figure not shown). Hence the model's atmospheric temperature response to the aerosol forcing has little dependence on the type of SST used. A maximum warming of about 2.5°C occurred in the lower stratosphere in the middle of 1992. When the model is forced by SST anomalies (Figure 6b, SI:SSTA), the simulated atmospheric temperature anomalies are small in the stratosphere. In the troposphere the simulated temperature increased by 0.1°C–0.3°C in JJA 1991 and MAM 1992 and decreased by 0.2°C in DJF 1992–1993. Results from the experiment SI:SSTA/VOL are quite similar to Figure 6b and are not shown. For the experiment SI:VOL + SSTA (Figure 6c), which includes both the Pinatubo aerosol and the SST anomalies, the simulated temperature changes in the stratosphere are primarily caused by the Pinatubo aerosol and look like those in Figure 6a, which include only the Pinatubo aerosol. In the troposphere both the Pinatubo aerosol and the SST forcing contributed to the simulated temperature anomalies, with the latter being dominant. *Kirchner and Graf* [1995] also found in their perpetual-January simulations that El Niño signals can be more clearly detected in the troposphere than in the stratosphere and that volcano signals are the strongest in the stratosphere.

[31] Figure 6d shows that the model overestimated the observed warming in the lower stratosphere when forced by both the Pinatubo aerosol and the SST anomalies and underestimated the observed cooling in the troposphere in 1992 and 1993. Large discrepancies up to +1.0°C ∼ +1.5°C are found in the middle of 1992 in the lower stratosphere. Additional numerical experiments and data analyses are presented in section 5 to further explore this discrepancy. It is noticeable that the model also slightly underestimated the observed warming in the lower stratosphere during a few months immediately after the Pinatubo eruption. This is probably because the prescribed aerosol optical properties accounted only for the sulfate aerosol particles and did not include the large amount of volcanic ash injected into the stratosphere. This ash returned to the Earth's surface under gravitational settling in no more than a few months [*McCormick et al.*, 1995]. Volcanic ash can absorb upwelling terrestrial radiation and warm the lower stratosphere.

[32] We further examine the geographic distributions of atmospheric temperature anomalies. Figure 7 shows the latitude-time distributions of zonal-mean monthly mean temperature anomalies at 50 hPa from June 1991 to May 1993 for the reanalysis and for the two ensemble experiments SI:VOL + SSTA and SI:SSTA. We present results at 50 hPa because the simulated maximum warming

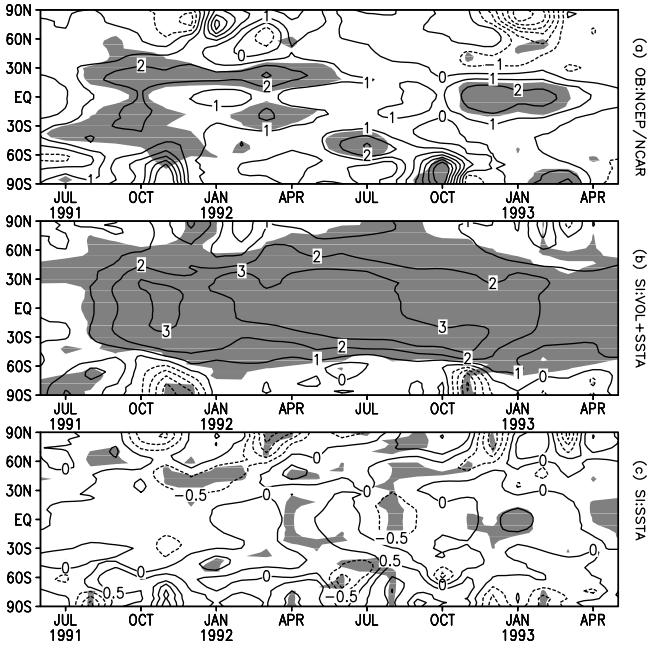

Figure 7. Monthly mean zonal-mean temperature anomalies at 50 hPa for (a) the NCEP/NCAR reanalysis and the simulations by the experiments (b) SI:VOL + SSTA and (c) SI:SSTA. For the NCEP/NCAR reanalysis, temperature anomalies larger than 1.3σ in magnitude are shaded, where σ is the standard deviation of zonal-mean temperature anomalies during 1950–1997. For the simulations, areas with statistical significance at or below the 10% level for a two-tailed *t*-test are shaded. The contour intervals are 1°C in Figures 7a and 7b and 0.5°C in Figure 7c. Dashed lines are negative anomalies. Solid lines are positive anomalies.

by the 24-layer ST-GCM occurs at this level. At 50 hPa the observed temperature (Figure 7a) was about 1°C–2°C higher than normal in the tropics and subtropics during most of the two years following the Pinatubo eruption. Between 10°N and 30°N a persistent and statistically significant large warming existed from August 1991 to April 1992. In the tropics the temperature anomaly was about +1°C to +2°C from August 1991 to March 1992, reduced to less than +1°C in the middle of 1992, and then increased again to about +2°C in DJF 1992–1993. The magnitude of the temperature anomalies in the tropics varied with time in part due to the dispersion of the Pinatubo aerosol cloud and in part due to the influence of the QBO [*Angell*, 1997b]. For the ensemble experiment SI:VOL + SSTA (Figure 7b) the simulated temperature anomaly in the subtropics and middle latitudes is about +1°C larger than observed for all months. In the tropics the simulated temperature anomaly is slightly larger than observed before January 1991, slightly smaller than observed after October 1992, and about 2°C larger than observed from February to September 1992. Additional experiments and analyses are presented in section 5 to determine how much of these discrepancies can be explained by the influences of the QBO and the observed ozone depletion. For the ensemble experiment SI:SSTA (Figure 7c) the ensemble-mean temperature anomaly is everywhere less than ±0.5°C except near the poles and is not statistically significant. The signal of SST anomalies in the stratosphere is weak compared to the signal of the volcanic aerosol forcing.

[33] *Kirchner et al.* [1999] and *Ramachandran et al.* [2000] also performed ensemble simulations using the ECHAM4 and SKYHI GCMs to examine the climatic impact of the Pinatubo eruption. Maximum zonal-mean temperature anomalies in the tropical stratosphere simulated by our 24-layer ST-GCM (Figure 7b) are close to those simulated by the SKYHI model [*Ramachandran et al.*, 2000, Figure 7a] in 1991 and about 1°C larger in 1992, and are about 1°C smaller than those simulated by the ECHAM4 model [*Kirchner et al.*, 1999, Figure 4a] in both years. Some of the differences can be attributed to model clouds and the layers where the largest aerosol optical depths are prescribed in the model [*Ramachandran et al.*, 2000]. Since the heating and cooling rates are almost the same among the three GCM simulations, it is probable that model responses to the Pinatubo aerosol forcing are sensitive to the model's vertical resolution, which can affect the vertical propagation of waves.

[34] Figure 8 is the same as Figure 7 except for temperature anomalies at 500 hPa. Neither the simulated nor the observed temperature anomaly is everywhere statistically significant. For both the experiment SI:VOL + SSTA and the NCEP/NCAR reanalysis, warming occurred before July 1992 and cooling occurred after July 1992 in the tropics. SST forcing contributed most to the temperature anomalies in the tropics. In the middle and high latitudes, both the simulated and the observed temperature anomalies exhibit large variations in time and in latitude and are statistically insignificant most of the time.

5. Influence of the QBO and Ozone Depletion

[35] In section 4 we found that the simulated temperature anomalies forced by the Pinatubo aerosol, no matter with climatological SST or real-time SST as boundary conditions, are about 1°C–2°C larger than observed in the middle of 1992 in the tropical lower stratosphere. Large biases are also found in the polar regions. In this section we show that the discrepancy can be explained in part by the QBO and ozone depletion, which are not resolved by our numerical simulations. *Kirchner et al.* [1999] estimated the influence of the QBO using composite analysis and the influence of ozone using the ECHAM4 GCM by prescribing in the model certain observations of ozone depletion. Here we extend the estimates using different approaches.

5.1. QBO

[36] Associated with the quasi-biennial oscillation of the equatorial zonal wind in the tropical lower stratosphere, there is a quasi-biennial oscillation of temperature [*Angell*, 1997a]. This temperature oscillation results from both the dynamical effect of the QBO and the radiative effect of the ozone oscillation that is linked to the QBO [*Angell*, 1997b]. However, the UIUC 24-layer ST-GCM did not simulate the QBO [*Yang et al.*, 2000]. Here we estimate the temperature anomalies in the tropical lower stratosphere associated with the QBO after the Pinatubo eruption using the NCEP/NCAR reanalysis.

[37] We present in Figure 9a the high-pass-filtered monthly mean temperature anomalies with timescales less than 120 months between 12°S and 12°N at 50 hPa from January 1958 to December 1998, together with the zonal-mean zonal wind at 30 hPa at the equator. The latter has been standardized and scaled to have the standard deviation of the temperature anomalies. We tested and found that compared to those on other isobaric surfaces, the zonal wind at 30 hPa best matches the phase change of the 50-hPa temperature anomaly. The two time series exhibit a close relation. A linear regression between the two time series is established by using the 30 years of data from January 1958 to December 1987 (Figure 9b). The correlation coefficient of the regression is 0.67. Using this statistical model, the temperature anomalies associated with the QBO after January 1988 are predicted by using the scaled zonal-mean zonal wind as predictor. Figure 9c depicts the predicted QBO-related temperature anomalies at 50 hPa, averaged between 12°S and 12°N, together with the observed high-pass-filtered temperature anomalies, the ensemble-mean temperature anomalies simulated by the experiment SI:VOL + SSTA, and the ensemble-

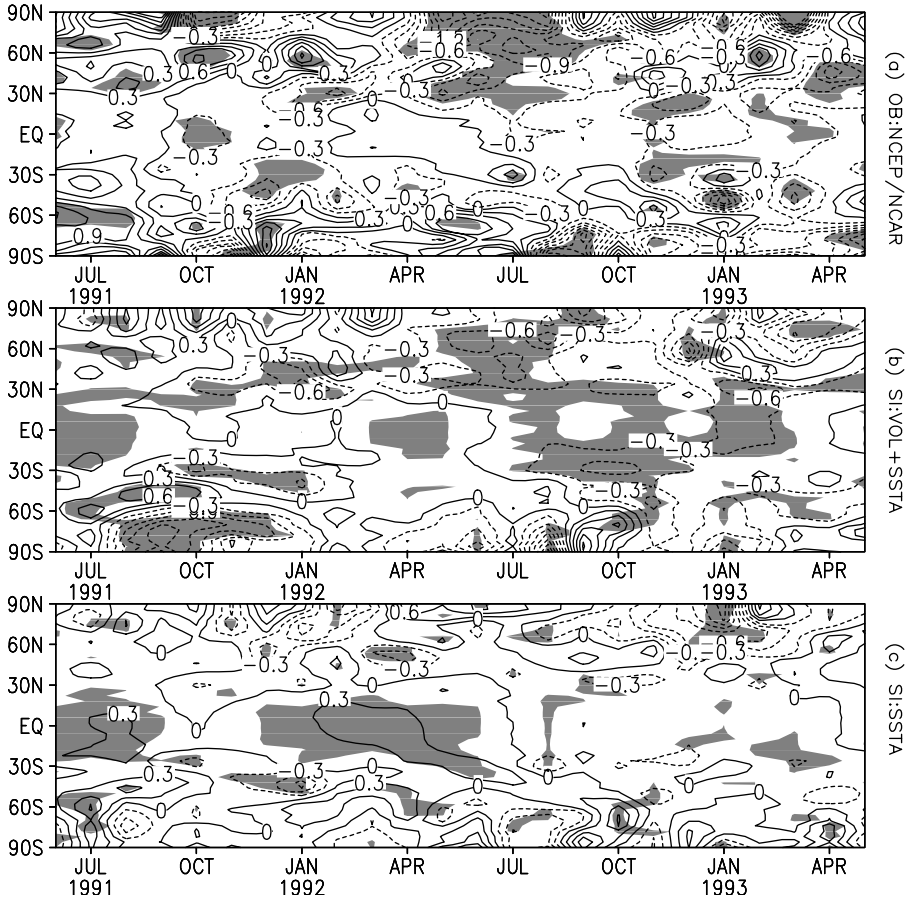

Figure 8. As in Figure 7 except for temperature anomalies at 500 hPa. The contour interval is 0.3°C in all panels.

mean temperature anomalies adjusted for the QBO. The Pinatubo eruption occurred during a transition time of the QBO from westerly phase to easterly phase. Following the eruption, the QBO was in an easterly phase before JJA 1992 and in a westerly phase after JJA 1992. Correspondingly, the QBO-related temperature anomaly predicted by the linear regression model was about −1.0°C before JJA 1992 and 1.0°C after JJA 1992. This QBO-related temperature oscillation explains in part the discrepancy between the observed and the simulated temperature anomalies in the tropical lower stratosphere. The remainder of the unexplained discrepancy is in part due to the radiative effect of ozone depletion caused by the volcanic aerosol.

5.2. Ozone Depletion

[38] Satellite observations revealed substantial total ozone losses over the globe for a few years following the Pinatubo eruption. *Randel et al.* [1995] showed that in the tropics, with the effect of the QBO excluded, the zonally averaged total ozone loss was initially about 4% in SON 1991 and about 2–3% throughout 1992 and 1993. In normal years the column total ozone varies by ±2–4% in the tropics, almost synchronously with the quasi-biennial oscillation of the equatorial zonal wind [*Bowman*, 1989]. In the Northern Hemisphere, poleward of 60°N, the observed zonal-mean total ozone decreased by about 10% during February–March 1992, by about 12% in February–March 1993, extending from middle latitudes to the North Pole, and by about 4% throughout the rest of 1992 and 1993. In the Southern Hemisphere, large decreases of total ozone in excess of 10% were found in the high latitudes in the austral spring seasons for the three years following the Pinatubo eruption [*Randel et al.*, 1995].

[39] The Pinatubo volcanic aerosol was the major cause for these observed ozone losses. Several competing mechanisms were involved [*Kinnison et al.*, 1994; *Tie et al.*, 1994]. First, the absorption of solar and terrestrial radiation by the volcanic aerosol cloud radiatively warmed the atmosphere. This heating changed the atmospheric circulation, which in turn affected the meridional transport of trace gases, including ozone. Second, the backscattering of solar radiation by the aerosol cloud changed the photolysis rate of ozone, especially in the tropics. Third, the heterogeneous chemical reactions in the lower stratosphere were enhanced on the surface of the volcanic aerosol particles. The observed ozone losses after the Pinatubo eruption were primarily caused by the perturbations of the circulation and photolysis rates at the initial stage and predominately by the enhanced heterogeneous chemical reactions at a later time, especially in the polar-night regions.

[40] For the ensemble simulations presented in section 4, the 24-layer ST-GCM was run with a climatological ozone distribution. Ozone absorbs both solar radiation and terrestrial radiation. It is the major absorber of solar radiation in the stratosphere. To estimate the influence of the observed ozone depletion on the simulated atmospheric temperature, we need the distributions of ozone concentration changes resolved in space and time following the Pinatubo eruption. The observed column total ozone losses by satellites are not useful for GCM studies. Therefore we performed two ensemble experiments by prescribing in the model the percentage changes of ozone concentration following the Pinatubo eruption simulated by two different 2-D radiative-chemical transport (RCT) models.

[41] The first data set of ozone depletion was provided by X.-X. Tie (personal communication, 1998) at the National Center for

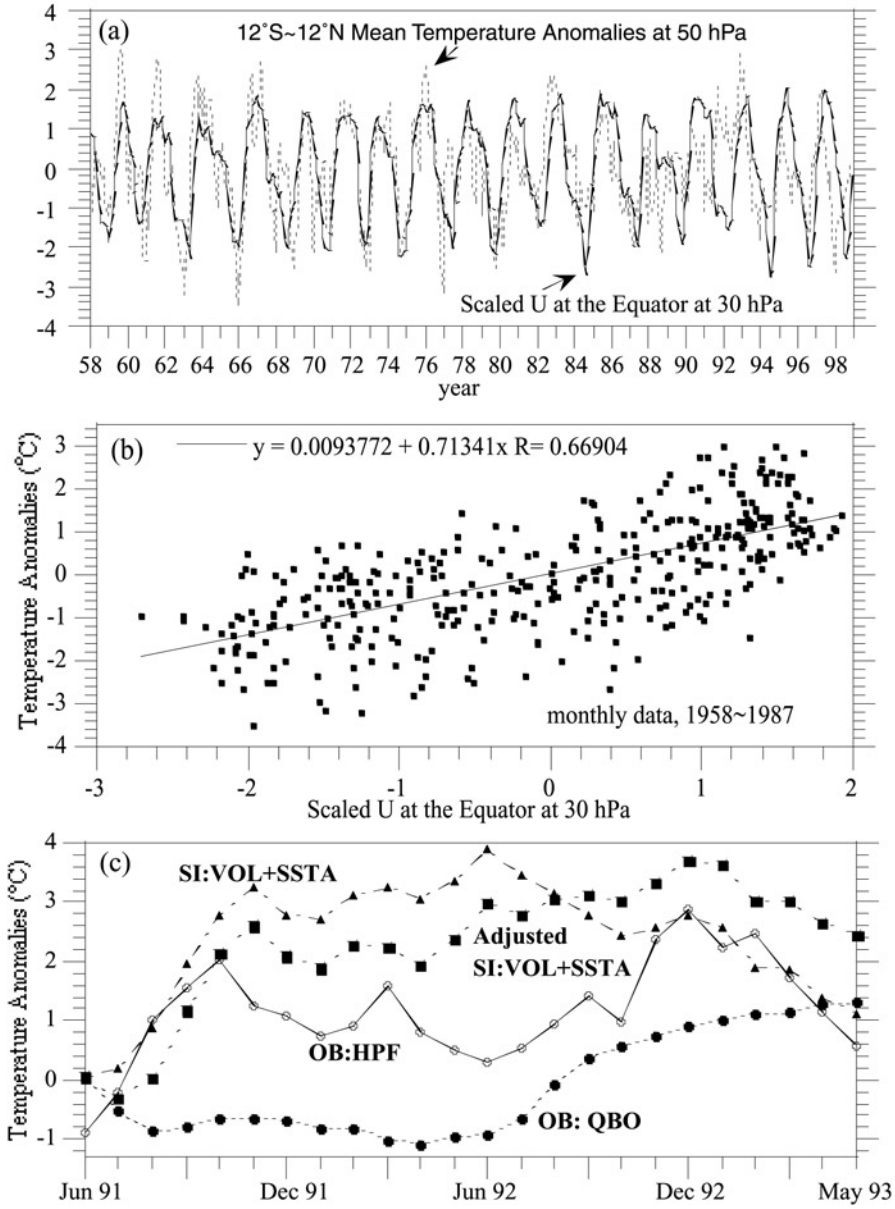

Figure 9. (a) High-pass-filtered monthly mean temperature anomalies between 12°S and 12°N at 50 hPa from January 1958 to December 1998 and the corresponding zonal-mean zonal wind at 30 hPa at the equator. The latter has been standardized and scaled to have the standard deviation of the temperature anomalies. (b). Scatterplot of the two time series in Figure 9a using their first 30 years of data and a linear regression. (c) Mean temperature anomalies between 12°S and 12°N from June 1991 to May 1993 for the high-pass-filtered observation (OB:HPF), the prediction by the regression model (OB:QBO), the simulation by the experiment SI:VOL + SSTA, and the simulation adjusted for the influence of the QBO (adjusted SI:VOL + SSTA).

Atmospheric Research (NCAR). Tie used the NCAR 2-D RCT model and the method of *Tie et al.* [1994]. This covers the time from June 1991 to May 1992. The effects of the Pinatubo aerosol on dynamical transport, photolysis rate, and chemical reactions were included. The simulated total ozone losses near the North Pole in early 1992 and in the tropics in late 1991 match the observations rather well. However, the model failed to simulate the observed ozone depletion in the Southern Hemisphere high latitudes. The simulated maximum ozone loss near 60°N descended too fast with height, from about 50 hPa in October 1991 to about 150 hPa in March 1992.

[42] K. Patten and D. Wuebbles at UIUC (personal communication, 1998 (hereinafter referred to as PW)) provided the second data set of ozone depletion. PW used the Lawrence Livermore National Laboratory 2-D RCT model [*Kinnison et al.*, 1994; *Patten et al.*, 1994]. They performed two 2-year-duration transient simulations, one with the aerosol surface area changing with time and the other with the aerosol surface area fixed to the value of 1990. In both simulations the atmospheric temperature and circulation were prescribed to be their climatological values and were not allowed to respond to any external forcing. Therefore the overloaded stratospheric aerosol

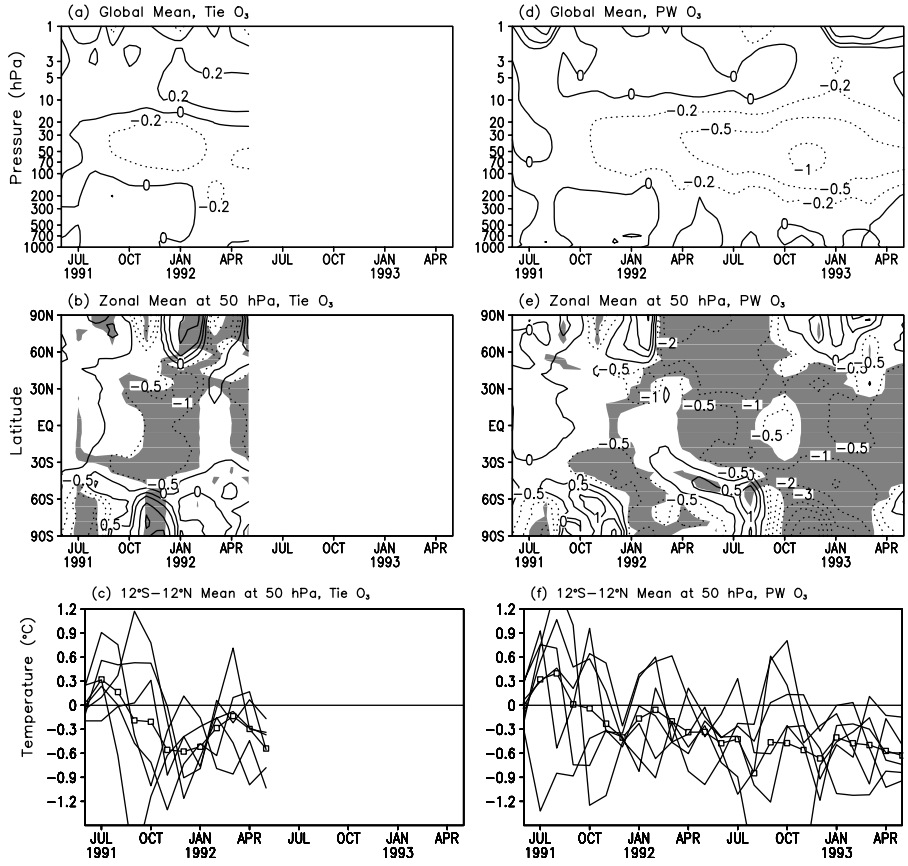

Figure 10. Temperature anomalies simulated by the 24-layer ST-GCM with prescribed ozone concentration changes from Tie (left) and PW (rights): (a, d) global-mean ensemble means, (b, e) zonal-mean ensemble means at 50 hPa, and (c, f) means between 12°S and 12°N at 50 hPa for the ensemble averages (solid lines with squares) and for each member of the ensemble (thin lines). (b, e) areas with statistical significance at or below the 10% level for a two-tailed *t*-test are shaded.

following the Pinatubo eruption was allowed to affect only the heterogeneous chemical reactions. This model captured the observed ozone losses in the Southern Hemisphere in the austral springs of 1991 and 1992. In the Northern Hemisphere the model also captured the observed large ozone losses in early boreal springs of 1992 and 1993. Probably, because of the lack of dynamical responses, the simulated ozone depletion is almost everywhere larger than observed, especially in the Northern Hemisphere middle to high latitudes in 1992 summer. In the tropics the simulated ozone losses are about 2–3% smaller than observed.

[43] We performed two 6-member ensemble simulations using the model initial conditions that have been used for the experiments in section 4, one from June 1991 to May 1992 and the other from June 1991 to May 1993, by prescribing in the UIUC 24-layer ST-GCM the percent changes of the zonally averaged ozone concentration simulated by the above 2-D RCT models. These simulations include Pinatubo aerosol and use real-time SSTs as boundary conditions; therefore results are compared to the experiment E4 in Table 1 to estimate the influences of ozone depletion on the simulated temperature anomalies. The time evolutions of the simulated ensemble-mean temperature anomalies by these two experiments are presented in Figure 10.

[44] In the first simulation year, the simulated maximum negative global-mean temperature anomalies are about −0.2°C with both Tie's and PW's ozone data (Figures 10a and 10d) in the lower stratosphere at the end of 1991. In the first few months after the Pinatubo eruption, the simulated temperature anomalies at 50 hPa in the tropics with Tie's ozone data (Figure 10b) are generally negative and are about −0.5°C to −1.0°C, while the simulated temperature anomalies with PW's ozone data (Figure 10e) are less than −0.5°C. This is because PW's simulation produced very small ozone depletion in the tropics. In the second simulation year from June 1992 to May 1993, the simulated global-mean temperature anomalies with PW's ozone data are between −0.5°C and −1.0°C, between 30 hPa and 100 hPa, with the largest cooling of about −1.0°C occurring at the end of 1992. In the tropics at 50 hPa the simulated temperature anomalies are between −0.5°C and −1.0°C. Larger coolings associated with ozone depletion are found at middle and high latitudes in both hemispheres. Figures 10c and 10f show that in the tropics (12°S–12°N), ozone depletion explains about 0.5°C temperature discrepancy found in Figure 9c between the simulations and observations at the end of 1991 and through 1992. Our estimate of ozone impact is much smaller than that of *Kirchner et al.* [1999], which is more than 1.0°C in DJF 1991–1992.

6. Summary

[45] Radiative forcing of the Pinatubo volcanic aerosol was calculated using the UIUC 24-layer ST-GCM for the two years following the eruption. Solar forcing is everywhere negative, and longwave forcing is everywhere positive. The calculated maxi-

mum negative global-mean net radiative forcing occurs in DJF 1991–1992, about −4.9 W/m^2 at the surface, −4.8 W/m^2 at the model top, and −5.6 W/m^2 at the tropopause. The forcing over cloudy sky is more than 2 W/m^2 smaller than over clear sky for all layers.

[46] Observational data analyses showed that during the two years following the Pinatubo eruption the temperature in the tropics and midlatitudes in both hemispheres was about 0.5°C–1.5°C higher than normal in the lower stratosphere and generally lower than normal in the troposphere.

[47] We performed four sets of ensemble simulations using the UIUC 24-layer ST-GCM to explore the thermal responses of the atmosphere to the Pinatubo aerosol forcing for the two years following the Pinatubo eruption. The model captured the observed surface warming in DJF 1991–1992 and DJF 1992–1993 over central North America and the observed surface cooling in JJA 1992 over both North America and Eurasia. The model did not capture the observed warming in DJF 1991–1992 over Eurasia. The simulated SAT anomalies are rather sensitive to the initial conditions and vary with the type of SSTs prescribed in the model. Overall, the simulation that is forced by both the Pinatubo aerosol and the observed SST anomalies best matches the observations. The simulation that is forced only by the SST anomalies well reproduced the observed SAT anomalies over land which can be attributed to the ENSO effect as estimated by SVD analysis.

[48] In the stratosphere the simulated temperature anomalies are not sensitive to the initial conditions and the magnitude of the simulated warming does not depend on the type of prescribed SSTs. The signal of SST anomalies in the stratosphere is rather weak compared to the Pinatubo aerosol forcing. In the troposphere the model captured the observed cooling. The simulated temperature anomalies are rather sensitive to the initial conditions and the type of prescribed SSTs. The signal of SST anomalies is stronger than the signal of the Pinatubo aerosol forcing in the troposphere.

[49] In the lower stratosphere the simulated temperature anomalies are about 1°C–1.5°C larger than observed in the tropics and subtropics in late 1991 and 1992. Part of the discrepancy is explained by the influences of the QBO and ozone depletion. In the tropical lower stratosphere the observed warming by the Pinatubo aerosol was diminished by up to 1°C before August 1992 and enhanced by up to 1°C after August 1992 by the QBO-related temperature changes. For the three years following the Pinatubo eruption, the observed total ozone decreased by 2–4% in the tropics and more than 10% in the high latitudes in both hemispheres in late winter and early spring times. The 24-layer ST-GCM was run with prescribed zonal-mean percent changes of ozone concentration, which were simulated by two different two-dimensional radiative-chemical transport models. Globally averaged, the simulated ensemble-mean temperature anomalies in the lower stratosphere induced by the ozone depletion are about −0.2°C in the first year and about −0.5°C to −1.0°C in the second year after the Pinatubo eruption.

[50] A discrepancy remains between the simulation and the observation, which is not explained by this study. The feedbacks among the QBO, ozone depletion, and atmospheric temperature and circulation are not resolved, and the roles of the oceanic thermal inertial and dynamics are not included.

[51] **Acknowledgments.** We thank two anonymous reviewers for their insightful suggestions and comments. This study was supported by the U.S. National Science Foundation (NSF) and the Carbon Dioxide Research Program, Environmental Sciences Division of the U.S. Department of Energy under grant ATM 95-22681, and by the NSF under grant ATM 00-0084270. Part of the computing time was provided by the Climate Simulation Laboratory of the National Center for Atmospheric Research and the National Energy Research Scientific Computing Center of the Department of Energy.

References

Andronova, N. G., E. Rozanov, F. Yang, M. E. Schlesinger, and G. L. Stenchikov, Radiative forcing by volcanic aerosols from 1850 through 1994, *J. Geophys. Res.*, *104*, 16,807–16,826, 1999.

Angell, J. K., Stratospheric warming due to Agung, El Chichón, and Pinatubo taking into account the quasi-biennial oscillation, *J. Geophys. Res.*, *102*, 9479–9485, 1997a.

Angell, J. K., Estimated impact of Agung, El Chichón and Pinatubo volcanic eruption on global and regional total ozone after adjustment for the QBO, *Geophys. Res. Lett.*, *24*, 647–650, 1997b.

Bowman, K. P., Global patterns of the quasi-biennial oscillation in total ozone, *J. Atmos. Sci.*, *46*, 3328–3343, 1989.

Graf, H. F., I. Kirchner, A. Robock, and I. Schult, Pinatubo eruption winter climate effects: Model versus observations, *Clim. Dyn.*, *9*, 81–93, 1993.

Groisman, P. Y., Possible regional climate consequences of the Pinatubo eruption: An empirical approach, *Geophys. Res. Lett.*, *19*, 1603–1606, 1992.

Hansen, J., A. Lacis, R. Ruedy, and M. Sato, Potential climate impact of Mount Pinatubo eruption, *Geophys. Res. Lett.*, *19*, 215–218, 1992.

Kinnison, D. E., K. E. Grant, P. S. Connell, D. A. Rotman, and D. J. Wuebbles, The chemical and radiative effects of the Mount Pinatubo eruption, *J. Geophys. Res.*, *99*, 25,705–25,731, 1994.

Kirchner, I., and H. F. Graf, Volcanoes and El Niño: Signal separation in Northern Hemisphere winter, *Clim. Dyn.*, *11*, 341–358, 1995.

Kirchner, I., G. L. Stenchikov, H. F. Graf, A. Robock, and J. C. Antuña, Climate model simulation of winter warming and summer cooling following the 1991 Mount Pinatubo volcanic eruption, *J. Geophys. Res.*, *104*, 19,039–19,055, 1999.

Knight, J. R., J. Austin, R. G. Grainger, and A. Lambert, A three-dimensional model simulation of the impact of Mt. Pinatubo aerosol on the Antarctic ozone hole, *Q. J. R. Meteorol. Soc.*, *124*, 1527–1558, 1998.

Kumar, A., and M. P. Hoerling, Annual cycle of Pacific-North America seasonal predictability associated with different phases of ENSO, *J. Clim.*, *11*, 3295–3308, 1998.

McCormick, M. P., L. W. Thomason, and C. R. Trepte, Atmospheric effects of the Mt Pinatubo eruption, *Nature*, *373*, 399–404, 1995.

Minnis, P., E. F. Harrison, L. L. Stowe, G. G. Gibson, F. M. Denn, D. R. Doelling, and W. L. J. Smith, Radiative climate forcing by the Mount Pinatubo eruption, *Science*, *259*, 1411–1415, 1993.

Parker, D. E., H. Wilson, P. D. Jones, J. R. Christy, and C. K. Folland, The impact of Mount Pinatubo on worldwide temperatures, *Int. J. Climatol.*, *16*, 487–497, 1996.

Patten, K. O., Jr., P. S. Connell, D. E. Kinnison, D. J. Wuebbles, T. G. Slanger, and L. Froidevaux, Effect of vibrationally excited oxygen on ozone production in the stratosphere, *J. Geophys. Res.*, *99*, 1211–1224, 1994.

Pudykiewicz, J. A., and A. P. Dastoor, On numerical simulation of the global distribution of sulfate aerosol produced by a large volcanic eruption, *J. Clim.*, *8*, 464–473, 1995.

Ramachandran, S., V. Ramaswamy, G. L. Stenchikov, and A. Robock, Radiative impact of the Mount Pinatubo volcanic eruption: Lower stratospheric response, *J. Geophys. Res.*, *105*, 24,409–24,429, 2000.

Randel, W. J., F. Wu, J. M. Russell III, J. W. Waters, and L. Froidevaux, Ozone and temperature changes in the stratosphere following the eruption of Mount Pinatubo, *J. Geophys. Res.*, *100*, 16,753–16,764, 1995.

Robock, A., Volcanic eruptions and climate, *Rev. Geophys.*, *38*, 191–219, 2000.

Robock, A., and J. Mao, The volcanic signal in surface temperature observations, *J. Clim.*, *8*, 1086–1103, 1995.

Russell, P. B., et al., Global to microscale evolution of the Pinatubo volcanic aerosol, derived from diverse measurements and analyses, *J. Geophys. Res.*, *101*, 18,745–18,763, 1996.

Sato, M., J. E. Hansen, M. P. McCormick, and J. B. Pollack, Stratospheric aerosol optical depths, 1850–1990, *J. Geophys. Res.*, *98*, 22,987–22,994, 1993.

Stenchikov, G. L., I. Kirchner, A. Robock, H.-F. Graf, J. C. Antuña, R. G. Grainger, A. Lambert, and L. Thomason, Radiative forcing from the 1991 Mount Pinatubo volcanic eruption, *J. Geophys. Res.*, *103*, 13,837–13,857, 1998.

Stowe, L. L., R. M. Carey, and P. P. Pellegrino, Monitoring the Mt. Pinatubo aerosol layer with NOAA/11 AVHRR data, *Geophys. Res. Lett.*, *19*, 159–162, 1992.

Tie, X., G. P. Brasseur, B. Briegleb, and C. Granier, Two-dimensional simulation of Pinatubo aerosol and its effect on stratospheric ozone, *J. Geophys. Res.*, *99*, 20,545–20,562, 1994.

Wang, W., Use of the UIUC 11-layer atmospheric general circulation model to simulate and understand the tropical intraseasonal oscillation, Ph.D. dissertation, 243 pp., Univ. of Ill., Urbana-Champaign, 1996.

Wang, W., and M. E. Schlesinger, The dependence on convection parameterization of the tropical intraseasonal oscillation simulated by the UIUC 11-layer atmospheric GCM, *J. Clim.*, *12*, 1423–1457, 1999.

Yang, F., Radiative forcing and climatic impact of the Mount Pinatubo volcanic eruption, Ph.D. dissertation, 219 pp., Univ. of Ill., Urbana-Champaign, 2000.

Yang, F., and M. E. Schlesinger, Identification and separation of Mount Pinatubo and El Niño-Southern Oscillation land surface temperature anomalies, *J. Geophys. Res.*, *106*, 14,757–14,770, 2001.

Yang, F., M. E. Schlesinger, and E. Rozanov, Description and performance of the UIUC 24-layer stratosphere/troposphere general circulation model, *J. Geophys. Res.*, *105*, 17,925–17,954, 2000.

Zhao, J., R. P. Turco, and O. B. Toon, A model simulation of Pinatubo volcanic aerosols in the stratosphere, *J. Geophys. Res.*, *100*, 7315–7328, 1995.

M. E. Schlesinger, Climate Research Group, Department of Atmospheric Sciences, University of Illinois at Urbana-Champaign, 105 S. Gregory Street, Urbana, IL 61801, USA. (schlesin@atmos.uiuc.edu)

F. Yang, Climate Prediction Center, National Centers for Environmental Prediction, Camp Springs, MD 20746, USA.